

MAGNETIC FIELDS IN ELLIPTICAL GALAXIES:
AN OBSERVATIONAL PROBE OF THE FLUCTUATION DYNAMO ACTION

AMIT SETA,^{1,2} LUIZ FELIPPE S. RODRIGUES,^{3,2} CHRISTOPH FEDERRATH,¹ AND CHRISTOPHER A. HALES^{4,2}

¹*Research School of Astronomy and Astrophysics, Australian National University, Canberra, ACT 2611, Australia*

²*School of Mathematics, Statistics and Physics, Newcastle University, Newcastle Upon Tyne, NE1 7RU, UK*

³*Department of Astrophysics, Radboud University, Heyendaalseweg 135, 6525 AJ Nijmegen, Netherlands*

⁴*National Radio Astronomy Observatory, P.O. Box 0, Socorro, NM 87801, USA*

ABSTRACT

Fluctuation dynamos are thought to play an essential role in magnetized galaxy evolution, saturating within ~ 0.01 Gyr and thus potentially acting as seeds for large-scale mean-field dynamos. However, unambiguous observational confirmation of the fluctuation dynamo action in a galactic environment is still missing. This is because, in spiral galaxies, it is difficult to differentiate between small-scale magnetic fields generated by a fluctuation dynamo and those due to the tangling of the large-scale field. We propose that observations of magnetic fields in elliptical galaxies would directly probe the fluctuation dynamo action. This is motivated by the fact that in ellipticals, due to their lack of significant rotation, the conventional large-scale dynamo is absent and the fluctuation dynamo is responsible for controlling the magnetic field strength and structure. By considering turbulence injected by Type Ia supernova explosions and possible magnetic field amplification by cooling flows, we estimate expected magnetic field strengths of $0.2 - 1 \mu\text{G}$ in the centers of quiescent elliptical galaxies. We use a semi-analytic model of galaxy formation to estimate the distribution and redshift evolution of field strengths, tentatively finding a decrease in magnetic field strength with decreasing redshift. We analyse a historical sample of radio sources that exhibit the Laing-Garrington effect (radio polarization asymmetry in jets) and infer magnetic field strengths between $0.14 - 1.33 \mu\text{G}$ for a uniform thermal electron density and between $1.36 - 6.21 \mu\text{G}$ for the thermal electron density following the King profile. We examine observational techniques for measuring the magnetic field saturation state in elliptical galaxies, focusing on Faraday rotation measure grids, the Laing-Garrington effect, synchrotron emission, and gravitational lensing, finding appealing prospects for future empirical analysis.

Keywords: dynamo – magnetic fields – galaxies: magnetic fields – ISM: magnetic fields – galaxies: elliptical and lenticular, cD – techniques: polarimetric

1. INTRODUCTION

Magnetic fields are ubiquitous in galaxies and their presence is usually explained by the turbulent dynamo theory, a process by which the turbulent kinetic energy in the medium is converted into the magnetic energy (Brandenburg & Subramanian 2005; Federrath 2016; Rincon 2019). Fluctuation dynamo, a type of magnetohydrodynamic (MHD) dynamo, is produced by a turbulent flow (characterized by the hydrodynamic Reynolds number $\text{Re} = u_{\text{rms}}\ell_0/\nu$, where u_{rms} is the root-mean square velocity field, ℓ_0 is the driving scale of the turbulence and ν is the viscosity) and therefore fluctuates in time and space. A weak seed magnetic field in a turbu-

lent electrically conducting fluid either grows exponentially or decays. The field grows only when the magnetic Reynolds number ($\text{Re}_M = u_{\text{rms}}\ell_0/\eta$, where η is the magnetic resistivity) is greater than its critical value, $\text{Re}_M^{(\text{crit})}$. For fluctuation dynamos, the $\text{Re}_M^{(\text{crit})}$ is approximately around 100 (can be higher for highly compressible and supersonic flows; Federrath et al. 2014) whereas the estimated Re_M in spiral galaxies is of the order of 10^{18} (Brandenburg & Subramanian 2005). Thus, the fluctuation dynamo is expected to be active in galaxies. Initially, the field is weak and the effect of the magnetic field on the velocity flow is negligible (this is referred to as the kinematic fluctuation dynamo). When the field grows, the magnetic field becomes strong enough to react back on the flow via the Lorentz force. This alters the properties of the turbulent flow. Eventually, the magnetic field saturates due to the back reaction of the Lorentz force on the flow.

MHD theories predict that a fluctuation dynamo will arise practically in any turbulent medium (as long as $\text{Re}_M > \text{Re}_M^{\text{(crit)}}$). The negligible seed field in protogalaxies is amplified quickly (in about 10^7 yr in spiral galaxies) to magnetic field strengths (of the order of $1\text{--}10\ \mu\text{G}$) in near equipartition with the turbulent kinetic energy. The fluctuation dynamo amplified field exists at small scales (with largest scale of the order of the driving scale of turbulence, $\ell_0 \approx 100$ pc in disks of spiral galaxies) and it requires the mean-field dynamo (Ruzmaikin et al. 1988; Beck et al. 1996; Brandenburg & Subramanian 2005) to further amplify and order the field over the observed kpc scales in spiral galaxies (e.g. in M51; Fletcher et al. 2011). Besides turbulence, the mean field dynamo also requires large-scale galaxy properties such as rotation, velocity shear and density stratification. Fluctuation dynamo plays an important role in seeding the mean field dynamo. The fluctuation dynamo action is described in detail in Brandenburg & Subramanian (2005).

Besides fluctuation dynamo, small-scale magnetic fields in spiral galaxies can also be generated by tangling of the mean (or large-scale) field and compression by shocks (for further discussion of these mechanisms, see Appendix A in Seta et al. 2018). The magnetic field generated by compression due to shocks is possibly correlated with the gas density (Federrath et al. 2011, 2014). The small-scale magnetic field due to a fluctuation dynamo is spatially intermittent, whereas that due to the tangling of the mean field is presumably Gaussian in nature due to pervasive Gaussian turbulence. Thus, the fluctuation dynamo generated magnetic field also decides the small-scale structure of magnetic fields in galaxies. In this paper, we propose how studying magnetic fields in quiescent elliptical galaxies can serve as a probe of the fluctuation dynamo action and discuss ways about pursuing the same.

Considering the driving scale of the turbulence in the interstellar medium (ISM) of spiral galaxies within a range of $50\text{--}100$ pc (Ohno & Shibata 1993; Gaensler et al. 2005; Fletcher et al. 2011; Houde et al. 2013)¹, it would require a spatial resolution of $\lesssim 10$ pc to study the structure of small-scale magnetic fields in spiral galaxies. Such a resolution is extremely difficult to achieve with present-day telescopes and thus it is difficult to observationally differentiate between the magnetic field generated by a fluctuation dynamo and that due to the tangling of the mean field. In a magnetized turbulent environment like the ISM of spiral galaxies, the fluctuation dynamo action is physically the most plausible scenario for magnetic field amplification but we are yet to confirm this in a galactic environment. The existence of a fluctuation dynamo in galaxies is fundamental to the galactic dynamo theory. In

the absence of a fluctuation dynamo, the magnetic field in protogalaxies would be seeded with a much weaker field and then the mean-field dynamo would take much longer to amplify the field up to the value observed today (Ruzmaikin et al. 1988; Arshakian et al. 2009). Furthermore, the field generated by a fluctuation dynamo is important for low-energy cosmic ray propagation (Shukurov et al. 2017) and for interpretations of radio observations. Thus, it is important to find a clear observational probe of the fluctuation dynamo action.

With a motivation to probe the fluctuation dynamo action in a galactic environment, we consider magnetic fields in elliptical galaxies (slow rotators, as defined by the ATLAS^{3D} Project in Emsellem et al. 2011; Cappellari et al. 2011²). Unlike spirals, elliptical galaxies have a very small rotation rate (with rotation velocity of about $20\ \text{km s}^{-1}$ as compared to $200\ \text{km s}^{-1}$ in a typical spiral galaxy) and so a mean-field dynamo (conventional $\alpha\omega$ dynamo) action is unlikely. Moreover, these systems are not differentially rotating, so a magnetorotational instability generated large-scale field is also unlikely. However, a weak seed magnetic field can still be amplified by the fluctuation dynamo action due to the interstellar turbulence driven by supernova explosions and the random motions of stars and gas induced by galactic dynamics (Moss & Shukurov 1996). The resulting magnetic field can be further amplified by compression produced by cooling flows (Fabian 1994) in elliptical galaxies (Mathews & Brighenti 1997). This leads to a magnetic field which is non-Gaussian and spatially intermittent.

Thus, the detection and characterization of magnetic fields in elliptical galaxies would be a direct observational confirmation of the fluctuation dynamo action. Moreover, the observations can be compared with the theories of fluctuation dynamos to further understand the physics of magnetic field saturation, which is an unsolved problem (a few possible saturation mechanisms are discussed in Tobias et al. 2011; Seta et al. 2015; Rincon 2019; Seta et al. 2020). It is also unclear whether the dominant scale (at which the magnetic power is at its maximum) lies close to the resistive scale (Schekochihin et al. 2002, 2004) or whether it is in fact much larger (Subramanian 1999). The spatially intermittent structure of magnetic fields generated by a fluctuation dynamo has been studied both analytically (Zeldovich et al. 1990) and numerically (Wilkin et al. 2007; Seta et al. 2020) but lacks observational confirmation.

The structure of the paper is as follows. In Sec. 2 we discuss turbulence in elliptical galaxies and predict the magnetic field strength generated by that turbulence. In Sec. 3 we predict properties of magnetic fields in elliptical galaxies obtained from a semi-analytical cosmological simulation. In Sec. 4

¹ Some observational studies report even smaller values of ℓ_0 in the range $1\text{--}20$ pc (Minter & Spangler 1996; Haverkorn et al. 2008; Iacobelli et al. 2013).

² <http://www-astro.physics.ox.ac.uk/atlas3d/>

we predict properties of the rotation measure distribution and present results from numerical simulations to verify these predictions. In Sec. 5 we estimate the magnetic field strengths using the Laing-Garrington effect and also examine observational prospects for measuring the magnetic field properties in elliptical galaxies using existing and forthcoming radio telescopes. Finally, we conclude in Sec. 6.

2. MAGNETIC FIELDS IN ELLIPTICAL GALAXIES

2.1. Turbulence in the hot gas of elliptical galaxies

The source of hot gas in ellipticals can be internal or external to the galaxy. Internally, the hot gas can be due to outflows from evolved stars and Type Ia supernova explosions. Externally, some of the circumgalactic gas (expelled from the galaxy by winds driven by frequent Type II supernovae explosions at earlier stages of galactic evolution) can fall back into the galaxy, as well as the gas accreted from the galaxy group or cluster. The hot gas in elliptical galaxies is observed via its X-ray emission. The relationship between the X-ray luminosity L_X and optical luminosity (in B band) L_B of bright elliptical galaxies is observationally found to be $L_X \propto L_B^{2.2}$ (O’Sullivan et al. 2001). This confirms the non-stellar origin of the X-ray emission, otherwise the relationship would have been linear. From X-ray observations, gas mass can be inferred. The total mass of the hot gas is about 1–2% of the total stellar mass (Mathews & Brighenti 2003).

The turbulence in spiral galaxies which merge to form an elliptical galaxy decays. The numerical simulations of decaying three-dimensional isotropic turbulence in an isothermal gas suggests that the turbulent velocity u_{rms} decays as a power-law, $(t/t_0)^{-\eta_u}$, with the exponent η_u in the range 0.4–0.6 and t_0 being the eddy turnover time (Mac Low et al. 1998; Stone et al. 1998; Subramanian et al. 2006; Sur 2019). Considering η_u as 0.6, the rms turbulent velocity in the parent spiral galaxy, $u_{\text{rms}} \approx 10 \text{ km s}^{-1}$ decreases to 1 km s^{-1} in $5 \times 10^8 \text{ yr}$ (where the eddy turnover time is calculated as follows: $t_0 \approx \ell_0 / u_{\text{rms}} \approx 100 \text{ pc} / 10 \text{ km s}^{-1} \approx 10^7 \text{ yr}$). However, we aim to look for magnetic fields in quiescent elliptical galaxies, which probably had a major merger a few Gyr earlier, so the turbulence due to parent spirals must have significantly decayed by then. Also, there is a lower level of turbulence (as compared to the parent spiral galaxies) maintained in quiescent elliptical galaxies due to continuous energy injection by Type Ia supernovae explosions. This is also seen in observations. Each explosion of a Type Ia supernova enriches the medium with roughly $0.7 M_\odot$ of iron and iron abundance in the hot gas of ellipticals increases from the outskirts to the centre of the galaxy, where the density is highest, so the supernova activity is highest (Mathews & Brighenti 2003). Further, the observed iron abundance can be used to estimate the supernova explosion rate in ellipticals (10^{-3} yr^{-1}). The rates are a factor of ~ 3 lower than in spiral galaxies ($3 \times 10^{-2} \text{ yr}^{-1}$).

Thus, the turbulence decays immediately after the merger of spiral galaxies but then is maintained at a certain level by continuous energy injection by Type Ia supernova explosions in quiescent elliptical galaxies. Type Ia supernova explosions will drive irrotational turbulence (negligible vorticity) in the ISM of elliptical galaxies. But this irrotational turbulence interacts with the multiphase ISM (see Li et al. 2020, and references therein, for reasons justifying the presence of inhomogeneous, multiphase gas in ellipticals) to generate vortical motions required for the fluctuation dynamo action.

To estimate the properties of turbulence in elliptical galaxies, we closely follow Moss & Shukurov (1996)³ with two major changes. First, they consider two drivers of turbulence: supernova explosions and random star motions, whereas we only consider Type Ia supernova explosions since the length scales associated with random star motions would be much smaller than those due to supernova explosions. Secondly, they consider acoustic turbulence but we consider hydrodynamic turbulence, because Mathews & Brighenti (1997) showed that the acoustic modes will quickly decay and cannot maintain the pervasive turbulence.

2.2. Estimating the properties of the ISM turbulence in elliptical galaxies

X-ray observations suggest a temperature T of the order of 10^7 K for the diffuse interstellar gas in elliptical galaxies (Mathews & Brighenti 2003). This implies a sound speed $c_s \approx \sqrt{k_B T / m_p} \approx 300 \text{ km s}^{-1}$, where $k_B = 1.38 \times 10^{-16} \text{ erg K}^{-1}$ is the Boltzmann constant and $m_p = 1.67 \times 10^{-24} \text{ g}$ is the proton mass (assuming that most of the hot gas mass is dominated by protons). We now use the sound speed and Sedov–Taylor blast wave self-similarity solution (Ostriker & McKee 1988) to calculate the driving scale of the turbulence. The radius of a supernova remnant R as a function of time t is then

$$R = \left(\kappa \frac{E_{\text{SN}}}{\rho_0} \right)^{1/5} t^{2/5}, \quad (1)$$

where E_{SN} is the energy of a supernova explosion, ρ_0 is the average gas density of the ambient medium and $\kappa \sim 2$ for a monoatomic ideal gas. Now, the radius R is roughly equal to the driving scale of the turbulence ℓ_0 , when the velocity of the shock front is equal to c_s . Thus, $t \approx R / c_s$. This gives

$$\ell_0 \approx \left(\kappa \frac{E_{\text{SN}}}{\rho_0} \right)^{1/3} \frac{1}{c_s^{2/3}}. \quad (2)$$

Using $E_{\text{SN}} = 10^{51} \text{ erg}$, $\rho_0 = m_p n_0 = 1.67 \times 10^{-27} \text{ g cm}^{-3}$ (assuming an ambient number density, $n_0 = 10^{-3} \text{ cm}^{-3}$, For-

³ The method is also very similar to that in Shukurov (2004) and Mac Low & Klessen (2004) where turbulent properties of the interstellar medium are estimated for supernova explosions in spiral galaxies.

man et al. 1985) and $c_s = 300 \text{ km s}^{-1}$, we obtain $\ell_0 \simeq 300 \text{ pc}$. This scale is slightly larger than that in spiral galaxies ($\simeq 100 \text{ pc}$) because the ambient medium is less dense.

The supernovae survive longer in ellipticals as compared to the spirals, but their frequency is much lower and so they inject less turbulent kinetic energy in the medium. To calculate the turbulent velocity, we assume that about 1% of the total supernovae energy is converted to the kinetic energy of the turbulence (Dyson & Williams 1997). The rate at which supernovae inject energy into the medium can be balanced with the rate of gain of kinetic energy of the medium as

$$\frac{v_0^2}{\ell_0/v_0} \approx f \nu_{\text{SN}} E_{\text{SN}} M_{\text{gas}}^{-1}, \quad (3)$$

where v_0 is the turbulent velocity, f is the fraction of energy that is injected into the medium, ν_{SN} is the frequency of supernova explosions and M_{gas} is the mass of the hot gas. Using $\ell_0 = 300 \text{ pc}$, $f = 0.01$, $\nu_{\text{SN}} = 10^{-3} \text{ yr}^{-1}$ (Cappellaro et al. 1999), $E_{\text{SN}} = 10^{51} \text{ erg}$ and $M_{\text{gas}} = 10^{10} M_{\odot}$, we obtain $v_0 \simeq 2.5 \text{ km s}^{-1}$. This is lower than that in spiral galaxies ($\simeq 10 \text{ km s}^{-1}$).

The estimated driving scale of turbulence (300 pc) is roughly similar to that obtained in Moss & Shukurov (1996) (350 pc), but the turbulent velocity we get (2.5 km s^{-1}) is smaller than their estimate (60 km s^{-1}). This is because we consider that Type Ia supernova explosions drive hydrodynamic turbulence rather than the acoustic turbulence, which they assume. The acoustic turbulence decays very quickly due to relatively high viscosity in the ISM of elliptical galaxies. For a fully ionised gas, with electron number density n_e and temperature T , the viscosity ν based on the kinetic theory is estimated as (Brandenburg & Subramanian 2005)

$$\nu \simeq 6.5 \times 10^{22} \left(\frac{T}{10^6 \text{ K}} \right)^{5/2} \left(\frac{n_e}{1 \text{ cm}^{-3}} \right) \text{ cm}^2 \text{ s}^{-1}, \quad (4)$$

where we assumed Coulomb logarithmic factor of order unity. For the core for an elliptical galaxy, $n_e = 0.1 \text{ cm}^{-3}$ and $T = 10^7 \text{ K}$, we obtain $\nu \simeq 2 \times 10^{26} \text{ cm}^2 \text{ s}^{-1}$. The diffusive length scale $l_\nu = (\nu/t)^{1/2}$ in an eddy turnover time $t_0 = 300 \text{ pc}/2.5 \text{ km s}^{-1} \simeq 10^7 \text{ yr}$ is $3 \times 10^5 \text{ cm}$, which is much smaller than the driving scale ($\sim 300 \text{ kpc}$). Thus, high viscosity dissipates acoustic waves within a very short distance. Plasma effects due to the presence of magnetic fields can reduce the viscosity calculated via Eq. 4, but not significantly to account for such a large difference. Furthermore, the dissipation of acoustic waves might provide an additional heating mechanism for the medium (details of mechanism in Fabian et al. 2005; Zweibel 2020).

The driving scale of turbulence $\ell_0 \simeq 300 \text{ pc}$ and the rms velocity $v_0 \simeq 2.5 \text{ km s}^{-1}$ are global values calculated from average quantities close to the core of a typical ellip-

tical galaxy⁴. The eddy turnover time can be calculated as $t_0 \simeq \ell_0/v_0 \simeq 1.2 \times 10^8 \text{ yr}$. The typical value of magnetic Reynolds numbers can also be calculated. Spitzer resistivity η for a plasma at a temperature T can be estimated from (Brandenburg & Subramanian 2005):

$$\eta \simeq 10^4 \left(\frac{T}{10^6 \text{ K}} \right)^{-3/2} \text{ cm}^2 \text{ s}^{-1}, \quad (5)$$

where we assumed the Coulomb logarithmic factor of order unity. Using $T = 10^7 \text{ K}$, we obtain $\eta \simeq 3 \times 10^2 \text{ cm}^2 \text{ s}^{-1}$. For $\ell_0 = 300 \text{ pc}$ and $v_0 = 2.5 \text{ km s}^{-1}$, we obtain $\text{Re}_M = \ell_0 v_0 / \eta \simeq 10^{24}$. The estimated Re_M is considerably greater than $\text{Re}_M^{(\text{crit})}$ ($\simeq 10^2$), which is required for the fluctuation dynamo action. Even though the flow is very viscous, such a high magnetic Reynolds number ensures fluctuation dynamo action in random flows. Thus, it is reasonable to expect fluctuation dynamo-generated magnetic fields in elliptical galaxies.

Since the gas and stellar densities in elliptical galaxies vary with radius (usually the variation is described by the King profile with a central core radius, see Statler 2012) the properties of the ISM turbulence would also change. We, however, are interested mostly in the core region of the elliptical galaxies where the density of the hot gas and supernova activity are higher and thus the expected magnetic field strength and the probability for an unambiguous detection is also higher. The magnetic field strength may be further enhanced close to the core due to the compression by cooling flows.

2.3. Fluctuation dynamo action and further amplification by cooling flows

The rms value of fluctuation dynamo generated magnetic field b_{rms} is in near equipartition with the turbulent kinetic energy (Haugen et al. 2004; Federrath et al. 2011; Tzeferacos et al. 2018; Seta et al. 2020),

$$b_{\text{rms}} \approx 0.5(4\pi\rho)^{1/2} v_0, \quad (6)$$

where ρ is the density of the medium and v_0 is the turbulent velocity. This is probably representative of magnetic field strengths in the core of elliptical galaxies. In the core of a typical elliptical, with $\rho = 0.1 m_p = 1.67 \times 10^{-26} \text{ g cm}^{-3}$ (Forman et al. 1985) and $v_0 = 2.5 \text{ km s}^{-1}$ (as obtained in Sec. 2.1), we obtain $b_{\text{rms}} \simeq 0.2 \mu\text{G}$.

The gas in the centers of elliptical galaxies quickly loses its energy via X-ray emission. Since the central core cools quickly, the weight of the outer region will cause the surrounding material to flow inwards. This is referred to as the

⁴ The high values of turbulent velocities of around 100 km s^{-1} reported using X-ray observations (de Plaa et al. 2012; Ogorzalek et al. 2017) are for a much larger halo of the elliptical galaxy. Such high values of turbulent velocities can be due to interaction with the AGN at the center of an elliptical galaxy or the surrounding environment.

cooling flow (Fabian 1994). They can also be inferred from the observations of O VI line emission from elliptical galaxies (Bregman et al. 2001, 2005). The magnetic field would be further enhanced by such cooling flows due to compression. By flux conservation under spherically symmetric compression, the field strength b grows as $\rho^{2/3}$, where ρ is the gas density. In cooling flows, the density can be enhanced by a factor of 10 or more (Mathews & Brighenti 1997). Thus, the magnetic field with magnitude approximately equal to $0.2 \mu\text{G}$ can be further amplified to be around $1 \mu\text{G}$. Mathews & Brighenti (1997), using a detailed spherical cooling flow model, suggest a radial dependence for the magnetic field strength of the form $b(r) \propto (1-10) r^{-1.2} \mu\text{G}$. The radial dependence of thermal electron number density is $n_e(r) \propto 0.1 r^{-1.5} \text{cm}^{-3}$ (Mathews & Brighenti 2003). Thus, we do expect a significant Faraday rotation of the polarized light from the background radio sources passing through the elliptical galaxy in the front (further discussed in Sec. 4 and Sec. 5.1).

3. PREDICTIONS FROM COSMOLOGICAL SIMULATIONS

We used the GALFORM semi-analytic model of galaxy formation (Lacey et al. 2016) to estimate the expected distribution of magnetic field strengths in elliptical galaxies and its redshift evolution. We classify any galaxy as elliptical in GALFORM's output where the bulge-to-total luminosity ratio in the r -band $(B/T)_r > 0.5$ (see §4.2.3 of Lacey et al. 2016 and Benson & Devereux 2010 for details). For the purposes of the calculations in this section, the contents of the remainder disk components of the selected galaxies were ignored.

As earlier, we assume that the magnetic field is amplified by a fluctuation dynamo (no further amplification due to the cooling flows is considered in the present model), with a steady-state rms strength given by Eq. (6). For the sake of definiteness we compute the equipartition strength at the half-mass radius, $r_{1/2}$, of each individual elliptical galaxy. Thus,

$$b_{\text{rms}}|_{r=r_{1/2}} \quad (7)$$

$$= 11.6 \mu\text{G} \left(\frac{M_g}{10^{10} M_\odot} \right)^{1/2} \times \left(\frac{\sigma_{1/2}}{50 \text{ km s}^{-1}} \right) \left(\frac{r_{1/2}}{5 \text{ kpc}} \right)^{-3/2} \quad (8)$$

where we have assumed that the density follows a Hernquist (1990) profile, with M_g corresponding to the total gas mass of the elliptical galaxy, and $\sigma_{1/2}$ is the velocity dispersion at the half-mass radius.

Fig. 1 shows the predicted distribution of rms strength of the magnetic field at the half-mass radius of elliptical galaxies as a function of redshift (ignoring galaxies without any gas). For the same comoving volume, we find that at a larger redshift the typical rms strength of the magnetic fields in elliptical galaxies

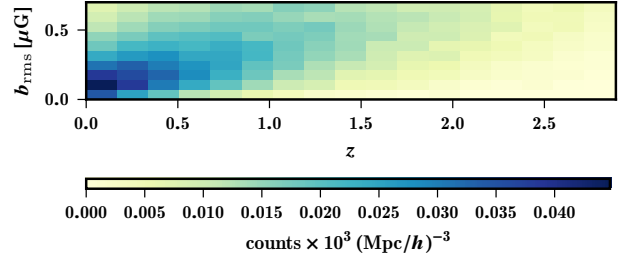


Figure 1. Redshift evolution of the distribution of b_{rms} at the half-mass radius of simulated elliptical galaxies with non-negligible gas content. Colors show the number of galaxies in each b_{rms} per comoving volume (where h is the Hubble parameter).

is larger than at lower redshifts, whereas the number of counts is expected to decrease. These trends follow the hierarchical assembly history of galaxies: the total number of elliptical galaxies increases with time, but the amount of available gas (and therefore, the typical field strength) decreases.

4. PROPERTIES OF FARADAY ROTATION MEASURE DISTRIBUTION FROM FLUCTUATION DYNAMO SIMULATIONS

4.1. Theoretical expectations for standard deviation of rotation measure fluctuations

The polarization angle of the linearly polarized synchrotron radiation rotates when the radiation passes through a magnetized medium containing thermal electrons. The amount of rotation is a function of the wavelength of the radiation and the Faraday rotation measure, RM, which in terms of convenient units is written as

$$\frac{\text{RM}}{1 \text{ rad m}^{-2}} = K \int_0^{L/1 \text{ pc}} \frac{n_e}{1 \text{ cm}^{-3}} \frac{b_{\parallel}}{1 \mu\text{G}} dl, \quad (9)$$

where n_e is the thermal electron number density, b_{\parallel} is the magnetic field parallel to the line of sight, L is the path length, and $K = 0.81$ when the units are scaled as indicated. For a cosmologically distant source at a redshift z , the RM in the observer frame is further reduced by a factor of $(1+z)^2$ than that given by Eq. 9 (which is the RM in the rest frame).

The standard deviation of fluctuations in rotation measure σ_{RM} can be estimated from the two-point correlation function of RM, which in turn can be estimated from the two-point correlation of the magnetic field. For the simplest case, this can be done by assuming that the number density of thermal electrons is uniform. Assuming a constant n_e in Eq. 9, Shukurov & Sokoloff (2007) demonstrated that

$$\frac{\sigma_{\text{RM}}}{1+z^2} = \frac{(2\pi)^{1/4}}{3^{1/2}} K n_e b_{\text{rms}} (L \ell_b)^{1/2}, \quad (10)$$

where b_{rms} is the root mean square magnetic field strength in the region, L is the path length and ℓ_b is the correlation

length of the random magnetic field. In the central region, assuming that the fluctuation dynamo is active (see Sec. 2.3), $n_e = 0.1 \text{ cm}^{-3}$ (Mathews & Brighenti 2003), $b_{\text{rms}} = 1 \mu\text{G}$, $\ell_b = 100 \text{ pc}$ ($\ell_0/\ell_b \approx 3\text{--}4$ and $\ell_0 \approx 300 \text{ pc}$), and $L = 10 \text{ kpc}$ (since the emission is considered close to the central region). For $z \approx 0$, these values yield $\sigma_{\text{RM}} \approx 75 \text{ rad m}^{-2}$. We expect that this can be observed in case of good signal to noise ratio. However, the number density decreases with the radius and this might further decrease the σ_{RM} at larger radii.

The analysis can be extended to include the contribution from a varying thermal electron number density (see Felten (1996) and Appendix A in Bhat & Subramanian (2013)). Assuming the King profile for electrons in an elliptical galaxy $n_e = n_e(0) (1 + (r/a)^2)^{-3/4}$, where $n_e(0)$ is the electron number density at $r = 0$, a is the core radius, and also assuming that $b_{\text{rms}} \propto n_e^\gamma$, σ_{RM} at $r = 0$ is

$$\frac{\sigma_{\text{RM}}(0)}{1 + z^2} = \frac{(2\pi)^{1/4}}{3^{1/2}} K n_e(0) b_{\text{rms}}(a\ell_b)^{1/2} \left(\frac{\Gamma\left(\frac{3}{2}(\gamma + 1) - 0.5\right)}{\Gamma\left(\frac{3}{2}(\gamma + 1)\right)} \right)^{1/2}. \quad (11)$$

Using $n_e(0) = 0.1 \text{ cm}^{-3}$, $b_{\text{rms}} = 1 \mu\text{G}$, $a = 3 \text{ kpc}$, $\ell_b = 100 \text{ pc}$, and $\gamma = 2/3$ (motivated by the flux freezing or cooling flow constraint, i.e., $b \propto \rho^{2/3}$), we obtain $\sigma_{\text{RM}}(0) \approx 35 \text{ rad m}^{-2}$ at $z \approx 0$. The σ_{RM} as a function of the radial distance in the plane of the sky r_\perp is

$$\sigma_{\text{RM}}(r_\perp) = \frac{\sigma_{\text{RM}}(0)}{1 + z^2} \left[1 + (r_\perp/a)^2 \right]^{-\left(\frac{1}{4} \Gamma\left(\frac{3}{2}(\gamma + 1) - 1\right) \right)}. \quad (12)$$

For $\sigma_{\text{RM}}(0)/(1 + z^2) = 35 \text{ rad m}^{-2}$ and $\gamma = 2/3$, we obtain $\sigma_{\text{RM}}(r_\perp) = 35 \text{ rad m}^{-2} (1 + (r_\perp/a)^2)^{-0.22}$.

Therefore, we expect significant fluctuations in Faraday rotation from at least the core of an elliptical galaxy (usually defined as the radius at which the slope of the surface brightness profile changes dramatically from low values).

4.2. Numerical simulations of fluctuation dynamo

We confirm our expectations for σ_{RM} using numerical simulations of the nonlinear fluctuation dynamo (numerically solving Navier-Stokes with a prescribed random forcing and induction equation for an isothermal gas in a periodic domain as described in Haugen et al. (2004)). The complete details of the simulations are described in Section II of Seta et al. (2020). The forcing is solenoidal, nearly incompressible and the Mach number of the flow is less than 0.1. We note that in numerical simulations of (Type Ia) supernova-driven turbulence, the overall Mach number is typically < 0.1 (Li et al. 2019). The initial conditions of our simulations are as follows: a uniform density, zero velocity, and a very weak random magnetic field with no net flux. As the turbulence is driven numerically within the domain, the density remains

roughly the same (since the gas is isothermal, the turbulent driving is near incompressible, and the Mach number is less than unity), and the velocity reaches a statistically steady state after about 2 turbulent eddy turnover times (e.g., Federrath et al. 2009; Price et al. 2011). The magnetic field first grows exponentially (kinematic stage) and then saturates (saturated stage) due to the back reaction of the flow via the Lorentz force induced by the magnetic field (Fig. 1 in Seta et al. 2020). We use the magnetic field from the saturated stage of the simulation with the forcing wavenumber $k_F = 5$, Reynolds number $\text{Re} = 283$ and magnetic Reynolds number $\text{Re}_M = 2261$ in a periodic box of non-dimensional size $L = 2\pi$ with 512^3 points (Seta et al. 2020). This means that there are 5 velocity correlation cells along each direction in the domain and a total of 125 cells in the whole cube. The simulations are for an isothermal gas with incompressible forcing. Thus, the electron number density is roughly uniform within the domain. To consider the effect of thermal electron number density distribution on the rotation measure distribution, we consider the following physically motivated distributions:

- a uniform n_e as suggested by isothermal simulations,
- n_e following the King profile similar to the gas density, i.e., $n_e(r) = n_e(0)(1 + (r/a)^2)^{-3/4}$, where a is the core radius,
- n_e proportional to $b^{3/2}$ as suggested by the magnetic flux freezing or cooling flow condition (extreme situation, ignores the turbulent nature of the medium).

We assume that the background polarized source density is uniform and the only effect the radiation has while passing through the simulation box is the rotation of its polarization angle, which is quantified by RM. With the fluctuation dynamo generated magnetic field b (normalized to $b_{\text{rms}} = 1$ over the numerical domain) for each n_e (normalized to $\langle n_e \rangle = 1$ over the numerical domain) given above, we calculate the RM at each point within a face of the domain as

$$\text{RM}(x_i, y_i) = K \sum_{i=1}^{512} n_e(x_i, y_i, z_i) b(x_i, y_i, z_i) dz, \quad (13)$$

where (x_i, y_i, z_i) is a coordinate on the grid and $dz = 2\pi/512$ is the grid spacing. This involves looking along the sightlines through the core of an elliptical galaxy and gathering statistics from the periodic box. We show the generated RM maps in Fig. 2 for all three cases: n_e constant (a), n_e King profile (b), and $n_e \propto b^{3/2}$ (c). The shape and size of structures for a constant n_e ((a) in Fig. 2) and for n_e following the King profile ((b) in Fig. 2) are very similar and for the King profile case, the intensity of RM decreases as a function of the distance from the center. For the third case, $n_e \propto b^{3/2}$ ((c) in Fig. 2), the structures are larger than in the other two cases, with very

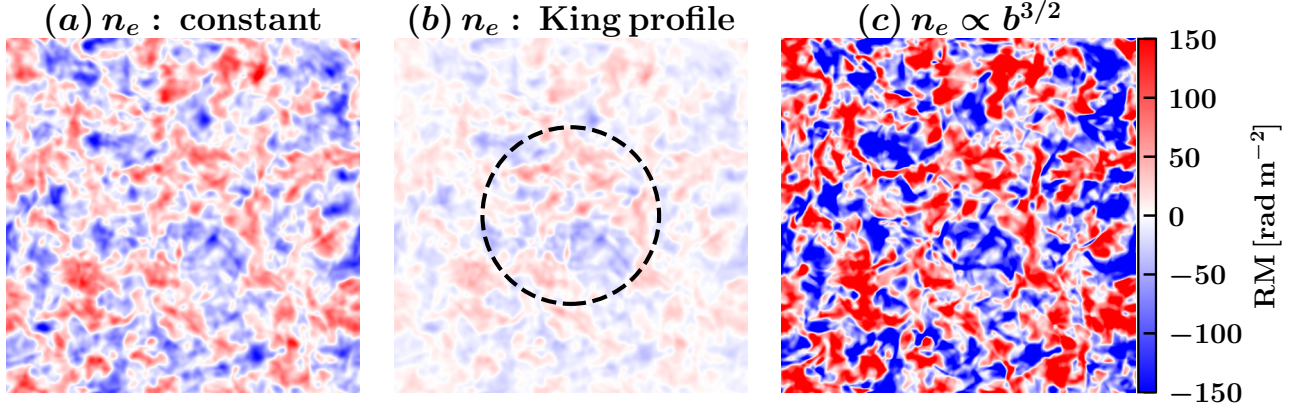


Figure 2. Two dimensional RM maps obtained using the intermittent magnetic field from a fluctuation dynamo simulation and three different electron number density distributions: (a) constant n_e , (b) n_e following the King profile, $n_e(r) = n_e(0)/(1 + (r/a)^2)^{-3/4}$, where $n_e(0)$ is the number density at the center, a is the core radius ($L/4$), and $r = ((x - L/2)^2 + (y - L/2)^2 + (z - L/2)^2)^{1/2}$ is the distance from the center, and (c) n_e from the flux-freezing or cooling-flow condition, $n_e \propto b^{3/2}$, where b is the field strength. The dotted, black circle in the case (b) shows the core radius $a = L/4$ in the King profile. For all three cases, over the entire numerical domain, the magnetic field is normalized to have a root mean square value of unity ($b/b_{\text{rms}} = 1$), and the mean thermal electron density is also normalized to unity ($\langle n_e \rangle = 1$). The structures in the cases (a) and (b) are very similar, except that the intensity of RM decreases as a function of r in the latter case. In case (c), the structures are different at smaller scales. The dynamo-generated magnetic field is exactly the same in all three cases, and the difference in the amplitude and the small-scale RM structures is due to different thermal electron distributions.

high RM values. On larger scales, the structures look similar for all three cases because of the same magnetic field, but the amplitude and small-scale RM structures vary depending on the n_e distribution.

4.3. Spectra and correlations function of rotation measure maps

Magnetic fields generated by nonlinear fluctuation dynamo simulations tend to follow a power-law spectrum with slope $3/2$ in the kinematic stage and $-5/3$ in the saturated stage (Fig. 2 in Seta et al. 2020). In Fig. 3(a), we show the one-dimensional (angle-integrated) power spectrum M_k of RM using the magnetic field in the saturated stage for the three different electron density distributions discussed above. The slope of the power spectra is similar for the constant n_e and n_e following the King profile case (red and blue lines in Fig. 3a), $k^{-0.8}$ and the power spectrum is much flatter for the case with $n_e \propto b^{3/2}$, $M_k \propto k^{-0.5}$. Even though all three cases have the same magnetic field, the RM power spectrum can be different. Then we calculate the second-order structure function $\text{SF}_{\text{RM}}(r)$ as (Monin & Yaglom 1971):

$$\text{SF}_{\text{RM}}(r) = \langle |\text{RM}(\mathbf{x} + \mathbf{r}) - \text{RM}(\mathbf{x})|^2 \rangle, \quad (14)$$

where \mathbf{x} is the position in the two-dimensional RM plane and $r = |\mathbf{r}|$ is the length of the displacement vector. Since we have periodic boundary conditions, we consider only half of the periodic domain, i.e., r varies from 0 to $L/2$. The scale at which the slope of the structure function of RM changes, referred to as the break scale, is usually related to the driving (or outer) scale of the turbulence (Haverkorn et al. 2008; Anderson et al. 2015). The structure function of RM can

be used to calculate the RM correlation function $C_{\text{RM}}(r)$ as (Hollins et al. 2017):

$$C_{\text{RM}}(r) = 1 - \frac{\text{SF}_{\text{RM}}(r)}{2\sigma^2}, \quad (15)$$

where $2\sigma^2$ is the value of SF_{RM} at which RM is no longer correlated, which would also be twice the standard deviation of RM, if there are a sufficient number of correlation cells in the numerical domain. The break scale can also be determined from the correlation function of RM. It is the length scale at which the correlation function crosses zero for the first time starting from $r = 0$. Fig. 3(b) shows the correlation function of RM for different electron density distributions. Even though the turbulence is driven on the same scale ($0.2L$) for all three cases, the break scale is different. The correlation length of RM can be calculated by integrating the correlation function as

$$\ell_b = \int C(r) dr. \quad (16)$$

Using Eq. 16, we calculate the correlation length of RM for all three cases and find $\ell_b/L = 0.125 \pm 0.07$, 0.080 ± 0.006 , and 0.052 ± 0.07 . For this analysis, we see that the correlation length depends not only on the thermal electron density distribution, but is also different from the break scale.

4.4. Probability distribution function of rotation measure maps

Fig. 4 shows the probability density function (PDF) of RM for the three electron number density distributions. In all cases, the mean RM ≈ 0 and the distribution is symmetric, because there is no large-scale field in the domain. Fig. 4(a)

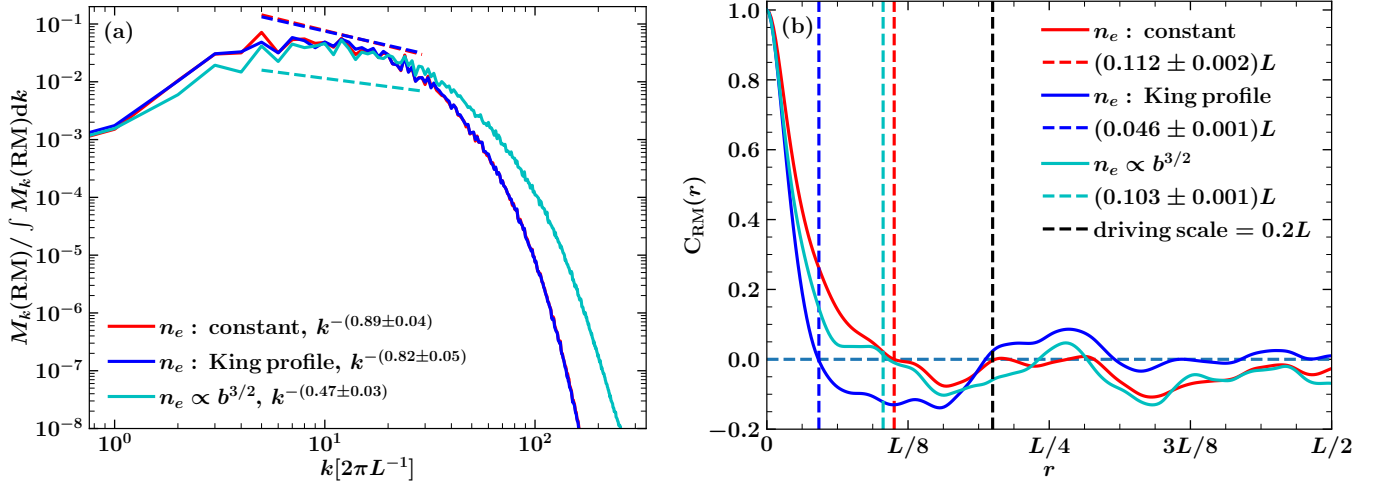


Figure 3. One-dimensional (angle-integrated) power spectrum $M_k(\text{RM})$ (a), and correlation function $C_{\text{RM}}(r)$ (b) of the RM maps shown in Fig. 2, for the same intermittent magnetic field obtained from a fluctuation dynamo simulation and three different thermal electron density distributions: constant n_e (red), n_e following the King profile (blue), and $n_e \propto b^{3/2}$ (cyan). In the range $3 \leq kL/2\pi \leq 20$ (in this range the magnetic field roughly follows a $k^{-5/3}$ power-law spectrum; see Fig. 2 of Seta et al. 2020), the constant n_e and n_e following the King profile cases have very similar slope, $k^{-0.8}$, whereas for the third case ($n_e \propto b^{3/2}$), the spectrum is flatter, $k^{-0.5}$ (dashed lines of the same color show the corresponding power-law approximations). The right-hand panel shows the correlation function for all three cases, and the dashed vertical lines show the break scale (slope of structure function changes first at this scale, thus referred to as a break scale). This break scale is usually related to the driving scale of the turbulence. However, the driving scale of the turbulence ($0.2L$) is the same for all three cases, and thus, the difference in break scales is due to the different thermal electron distributions.

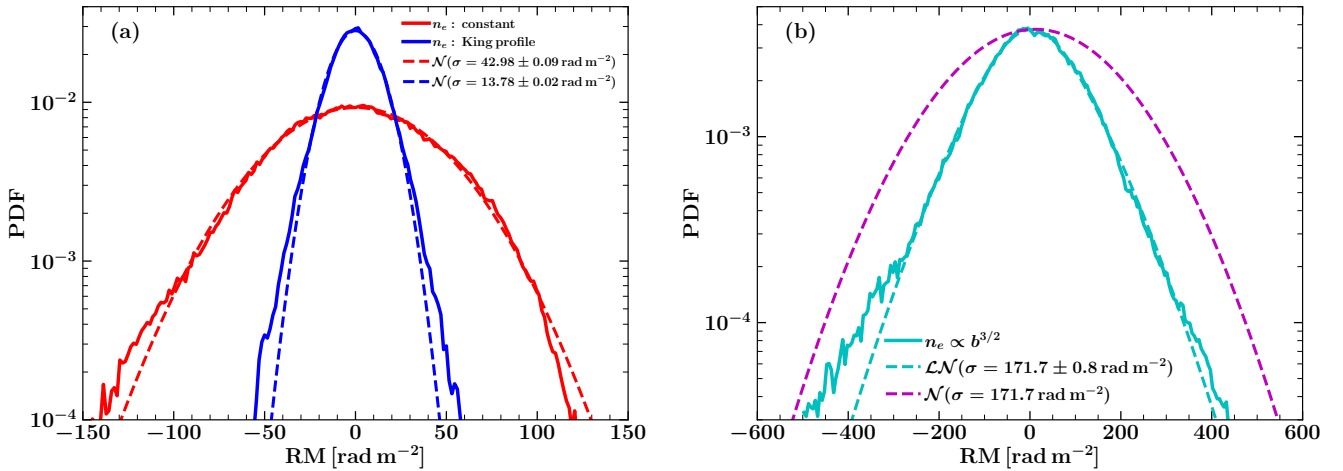


Figure 4. (a) PDFs of RM distribution for the cases where the electron number density n_e is not correlated to the magnetic field strength: n_e constant (red) and n_e following the King distribution (blue) with $a = L/4 = 1.25\ell_0$, where ℓ_0 is the driving scale of turbulence. Both distributions are roughly Gaussian (dashed lines of the same color show the corresponding fitted Gaussian distribution) with mean $\text{RM} \approx 0$ (since a mean magnetic field is absent). The standard deviation σ is lower for the King profile. (b) PDF of RM for the case where n_e is related to magnetic field strength b via the flux freezing or cooling flow condition, i.e., $n_e \propto b^{3/2}$. The distribution (cyan) is clearly non-Gaussian (the dashed-magenta line shows a Gaussian distribution with the same standard deviation as the fitted distribution) and can be approximated by a product of a Cauchy-Lorentz distribution and a Gaussian function (the dashed cyan line shows the fitted function). For the same magnetic field, the standard deviation and the shape of the RM distribution differs significantly due to different (physically motivated) thermal electron density distributions.

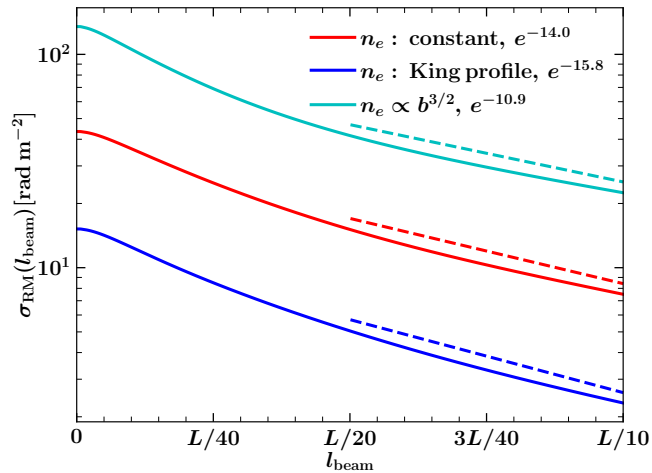


Figure 5. Standard deviation of RM, σ_{RM} , as a function of beam size l_{beam} for all three electron density distributions. The standard deviation decreases as the beam size increases, and the decrease is exponential for large l_{beam} . Even when the beam size is one-tenth of the numerical domain, the standard deviation between the three cases still differs significantly.

shows the PDFs for two distributions of n_e : uniform and following a King profile with $a = L/4 = 1.25\ell_0$. Both distributions are close to a Gaussian distribution (\mathcal{N}) with different standard deviations σ_{RM} . The one with the King profile has a smaller standard deviation. The distributions agree well with the analytical expressions, Eq. 10 and Eq. 11, respectively. Fig. 4(b) shows the RM distribution when $n_e \propto b^{3/2}$. The distribution is clearly non-Gaussian and can be approximated by a product of a Cauchy–Lorentz distribution and a Gaussian function (\mathcal{LN}). The Gaussian or non-Gaussian nature of the RM distribution in these cases follows from Eq. 9 or Eq. 13. In an isotropic random magnetic field, the polarization angle performs a random walk as it rotates randomly along the path length. When n_e does not depend on b directly, RM depends on the first power of the magnetic field and the random walk is a Brownian motion which gives rise to a Gaussian distribution. For the case where $n_e \propto b^{3/2}$, RM depends on a higher power of the magnetic field and since the underlying magnetic field is intermittent, the resulting RM distribution is non-Gaussian. In the case of a non-Gaussian distribution, it is difficult to associate a single number (for example σ_{RM}) to the distribution but the calculated standard deviation for a non-Gaussian distribution would be far higher than that for a Gaussian distribution (compare the x -axis in Fig. 4(a) and Fig. 4(b)). The calculated standard deviation of the RM distribution shown in Fig. 4(b) is approximately equal to 170 rad m^{-2} , whereas the deviation for both the Gaussian distributions in Fig. 4(a) is less than 100 rad m^{-2} . We show that the standard deviation of fluctuations in RM are significantly different for different thermal electron number density distributions for a given fixed magnetic field.

Furthermore, to account for the effects of beam smearing, we perform a Gaussian smoothing of the RM maps with a beam size (or smoothing scale) l_{beam} ranging from 0.0 (no smoothing) to $L/10$ (beam size one-tenth of the numerical domain). The dependence of the standard deviation of RM on l_{beam} is shown in Fig. 5. For all three cases of the thermal electron density distribution, σ_{RM} decreases (exponentially for high l_{beam}), but the difference between the three cases still persists even for strong smoothing of the RM maps.

Thus, the fluctuations in rotation measure should not be directly associated with the fluctuations in the magnetic fields without considering the fluctuations in thermal electron density. This sets an expectation for future observations.

5. OBSERVATIONAL PROSPECTS: MAGNETIC FIELDS USING THE LAING-GARRINGTON EFFECT

Observations of magnetic fields in elliptical galaxies are needed to assess the true magnetic field saturation state resulting from fluctuation dynamo action. Several possible approaches are outlined below. Selection effects are discussed in Section 5.5.

5.1. Rotation Measure Grid

The most direct approach would be to measure RM variance using a grid of polarized background radio sources observed through the ISM of a foreground elliptical galaxy. This requires a sufficient number of background sources to enable separation of RM fluctuations arising within and external to the target galaxy. This approach is unlikely to be feasible for any individual galaxy, even if using future highly sensitive radio telescopes, because the sky density of background polarized sources (e.g. Hales et al. 2014 and Fig. 3 from Hales 2013) will be too low to yield a sufficient statistical sample behind even an arcmin-sized galaxy (see Section 5.4 in Seta 2019, for an estimate to observe RMs from background extragalactic sources seen through the nearest elliptical galaxy Maffei 1). A more promising approach could be to identify elliptical galaxies located in the foreground of extended polarized radio sources (e.g. lobes), through which spatially-resolved RM fluctuations may even be discerned. Depolarization in this scenario would also yield constraints on σ_{RM} .

Similarly, polarized fast radio bursts (FRBs) could be used to gather RM statistics. The event rate of FRBs (e.g. Petroff et al. 2019; Cordes & Chatterjee 2019) is probably insufficient to sample many independent sightlines through any individual foreground galaxy within a realistic timeframe. Furthermore, it may be unrealistic to consider gathering statistics of host galaxy RM contributions to study ellipticals; while the emission mechanism(s) of FRBs and their identification with any particular astronomical object or phenomenon remain unknown, their compelling association with young neutron stars

(Metzger et al. 2019) and with environments that scatter radio waves (CHIME/FRB Collaboration et al. 2019) appear to argue against an origin within old stellar populations. Instead, a plausible approach might be to compare a control sample of RMs from FRBs with those located behind elliptical galaxies.

The approaches above could also be attempted without prior knowledge of the foreground elliptical galaxies by searching for correlations with various line tracers. For example, a similar correlation has been identified between polarization properties of background sources and Mg II absorption line systems, indicating a likely association with magnetic outflows from intervening star forming galaxies (Kim et al. 2016).

5.2. Laing-Garrington effect

Laing (1988) and Garrington et al. (1988) studied radio polarization from Fanaroff–Riley Class II (FR II) sources and observed that the level of fractional polarization was significantly higher on the jet side closer to us than on the counter-jet side pointing away from us. This is referred to as the Laing-Garrington effect. Assuming that both jets have similar intrinsic properties, the difference in fractional polarization can be attributed to depolarization by a foreground screen arising from the X-ray emitting halo of the elliptical galaxy, where the radiation from the more distant side travels more through the screen and is thus more depolarized.

If the elliptical galaxy acts as a Faraday screen, i.e. a medium with magnetic fields and thermal electrons but lacking relativistic electrons (this is a justified assumption since an elliptical galaxy has a scarcity of cosmic ray electrons), and if it is assumed that the jet does not significantly disturb the ISM, we can use historical observations of the Laing-Garrington to probe magnetic fields in elliptical galaxies. We investigate this observational approach below using available historical data.

For a Faraday screen, assuming a Gaussian distribution of Faraday depths, the degree of polarization p at wavelength λ is given by (Burn 1966; Sokoloff et al. 1998)⁵

$$p = p_0 \exp(-2\sigma_{\text{RM}}^2 \lambda^4), \quad (17)$$

where p_0 is the maximum degree of polarization and σ_{RM} is the standard deviation of the fluctuations in rotation measure due to the screen. The depolarization DP (see Fig. 7 in Basu et al. 2019, for DP calculated from MHD simulations) between the wavelengths λ_1 and λ_2 with $\lambda_1 > \lambda_2$ is given by

$$\text{DP} = \exp(-2\sigma_{\text{RM}}^2 (\lambda_1^4 - \lambda_2^4)). \quad (18)$$

⁵ This also assumes no foreground RM structure; see EnBlin & Vogt (2003); Murgia et al. (2004); Laing et al. (2008), for a discussion on its effect.

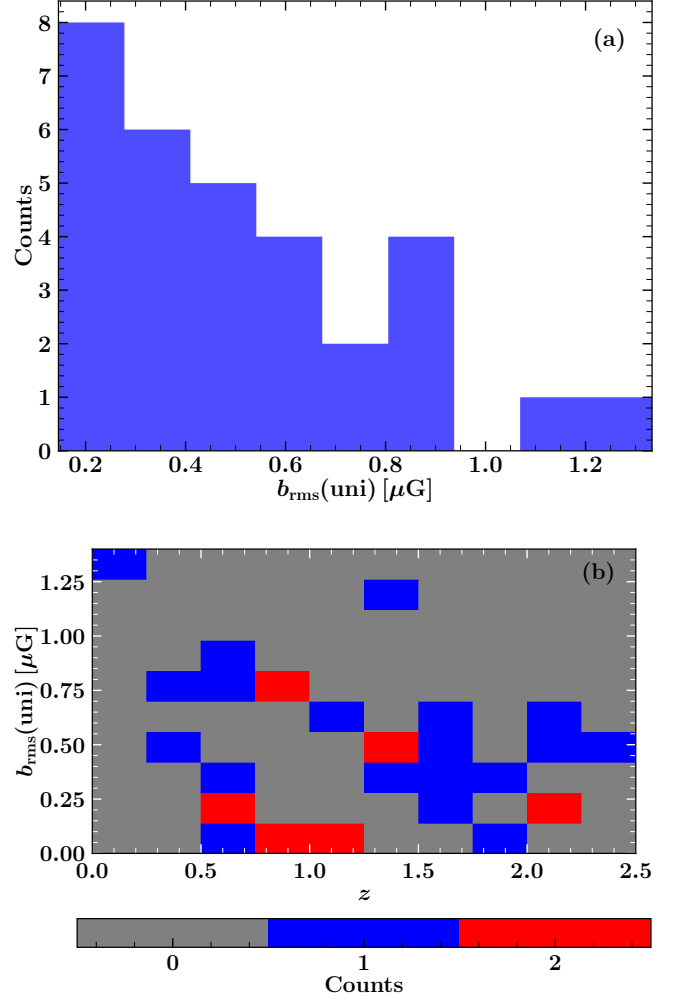


Figure 6. (a) Histogram of rms magnetic field strength $b_{\text{rms}}(\text{uni})$ [μG] obtained from the asymmetry in polarization properties of jets from sources associated with elliptical galaxies assuming a uniform thermal electron density $n_e = 10^{-2} \text{ cm}^{-3}$. (b) Two dimensional histogram of the redshift of the sources z and $b_{\text{rms}}(\text{uni})$. At lower z , b_{rms} is somewhat higher compared to that at the higher z values.

Using Eq. 18, we obtain the standard deviation in the rotation measure distribution for the jet σ_{RM_j} and counter jet $\sigma_{\text{RM}_{c_j}}$. Then, assuming that the difference is due to the halo of an elliptical galaxy, we derive the standard deviation in the rotation measure distribution for the galaxy $\sigma_{\text{RM}_{\text{ellip}}}$ from the standard deviation of rotation measure for the jet and counter jet as follows:

$$\sigma_{\text{RM}_{\text{ellip}}} = \sqrt{\sigma_{\text{RM}_{c_j}}^2 - \sigma_{\text{RM}_j}^2}, \quad (19)$$

Finally, the $\sigma_{\text{RM}_{\text{ellip}}}$ is used to estimate the magnetic field strength b_{rms} using the equation Eq. 10 for uniform thermal electron number density and Eq. 11 for the King profile.

Garrington & Conway (1991) did a similar estimate for a typical single source at low redshift and another source at a

Table 1. List of sources, their redshifts z , their projected linear size LS, the depolarization fraction for jets DP_j and counter jets DP_{cj} with their respective uncertainties (Garrington et al. 1991). The calculated standard deviation of the rotation measure in jets σ_{RM_j} , counter jets $\sigma_{RM_{cj}}$, elliptical hosts $\sigma_{RM_{ellip}}$, and the rms magnetic field in ellipticals with their respective uncertainties for the uniform n_e $b_{rms}(uni)$ and for the n_e following the King profile $b_{rms}(KP, r = 0)$ are also given.

Name	z	LS	DP_j	DP_{cj}	σ_{RM_j}	$\sigma_{RM_{cj}}$	$\sigma_{RM_{ellip}}$	$b_{rms}(uni)$	$b_{rms}(KP, r = 0)$
–	#	(kpc)	#	#	(rad m^{-2})	(rad m^{-2})	(rad m^{-2})	(μG)	(μG)
0017+15	2.012	88	0.61 ± 0.02	0.21 ± 0.07	12.48 ± 0.41	22.17 ± 2.37	18.33 ± 2.88	0.29 ± 0.05	1.82 ± 0.29
0123+32	0.794	192	0.96 ± 0.04	0.89 ± 0.03	3.59 ± 1.83	6.06 ± 0.88	4.88 ± 1.73	0.15 ± 0.05	1.36 ± 0.48
0225-01	2.037	131	0.85 ± 0.03	0.08 ± 0.04	7.16 ± 0.78	28.21 ± 2.79	27.29 ± 2.89	0.35 ± 0.04	2.66 ± 0.28
0232-04	1.436	110	0.81 ± 0.03	0.16 ± 0.05	8.15 ± 0.72	24.03 ± 2.05	22.60 ± 2.19	0.49 ± 0.05	3.42 ± 0.33
0838+13	0.684	89	0.73 ± 0.04	0.25 ± 0.02	9.96 ± 0.87	20.90 ± 0.60	18.37 ± 0.83	0.93 ± 0.04	5.83 ± 0.26
0850+58	1.322	129	0.57 ± 0.04	0.15 ± 0.03	13.31 ± 0.83	24.45 ± 1.29	20.51 ± 1.63	0.45 ± 0.04	3.42 ± 0.27
1023+06	1.699	112	0.45 ± 0.03	0.25 ± 0.06	15.86 ± 0.66	20.90 ± 1.81	13.61 ± 2.88	0.24 ± 0.05	1.68 ± 0.36
1115+53	1.235	77	0.86 ± 0.03	0.18 ± 0.04	6.89 ± 0.80	23.24 ± 1.51	22.20 ± 1.60	0.68 ± 0.05	4.00 ± 0.29
1218+33	1.519	79	0.56 ± 0.02	0.07 ± 0.04	13.52 ± 0.42	28.94 ± 3.11	25.60 ± 3.52	0.61 ± 0.08	3.63 ± 0.50
1226+10	2.296	40	0.69 ± 0.04	0.04 ± 0.02	10.81 ± 0.84	31.85 ± 2.47	29.95 ± 2.65	0.59 ± 0.05	2.48 ± 0.22
1241+16	0.557	116	0.90 ± 0.06	0.41 ± 0.04	5.76 ± 1.82	16.76 ± 0.92	15.74 ± 1.18	0.81 ± 0.06	5.84 ± 0.44
1258+40	1.659	172	0.84 ± 0.04	0.11 ± 0.05	7.41 ± 1.01	26.37 ± 2.72	25.31 ± 2.84	0.37 ± 0.04	3.22 ± 0.36
1318+11	2.171	37	0.97 ± 0.04	0.06 ± 0.06	3.10 ± 2.10	29.77 ± 5.29	29.61 ± 5.32	0.65 ± 0.12	2.65 ± 0.48
1323+65	1.618	71	0.73 ± 0.03	0.18 ± 0.03	9.96 ± 0.65	23.24 ± 1.13	21.00 ± 1.29	0.49 ± 0.03	2.75 ± 0.17
1634+17	1.897	55	0.77 ± 0.08	0.27 ± 0.07	9.07 ± 1.80	20.31 ± 2.01	18.17 ± 2.42	0.39 ± 0.05	1.95 ± 0.26
1634+58	0.985	73	0.84 ± 0.10	0.25 ± 0.04	7.41 ± 2.53	20.90 ± 1.21	19.54 ± 1.61	0.78 ± 0.06	4.46 ± 0.37
1656+57	1.281	33	0.90 ± 0.04	0.10 ± 0.10	5.76 ± 1.22	26.93 ± 5.85	26.31 ± 5.99	1.19 ± 0.27	4.55 ± 1.04
1709+46	0.806	103	0.56 ± 0.02	0.15 ± 0.03	13.52 ± 0.42	24.45 ± 1.29	20.37 ± 1.57	0.83 ± 0.06	5.62 ± 0.43
1732+16	1.270	132	0.68 ± 0.05	0.08 ± 0.04	11.02 ± 1.05	28.21 ± 2.79	25.97 ± 3.07	0.59 ± 0.07	4.53 ± 0.53
1816+47	2.225	49	0.82 ± 0.06	0.06 ± 0.03	7.91 ± 1.46	29.77 ± 2.65	28.70 ± 2.77	0.53 ± 0.05	2.48 ± 0.24
0107+31	0.689	364	0.65 ± 0.03	0.39 ± 0.02	11.65 ± 0.62	17.22 ± 0.47	12.69 ± 0.86	0.31 ± 0.02	4.00 ± 0.27
0712+53	0.064	49	0.34 ± 0.03	0.28 ± 0.03	18.44 ± 0.75	20.03 ± 0.84	7.82 ± 2.80	1.33 ± 0.48	6.21 ± 2.22
0824+29	0.458	129	0.86 ± 0.05	0.44 ± 0.02	6.89 ± 1.33	16.08 ± 0.45	14.53 ± 0.80	0.81 ± 0.04	6.15 ± 0.34
0903+16	0.411	280	0.65 ± 0.02	0.38 ± 0.03	11.65 ± 0.42	17.46 ± 0.71	13.00 ± 1.03	0.53 ± 0.04	5.87 ± 0.46
1001+22	0.974	576	0.50 ± 0.04	0.36 ± 0.02	14.78 ± 0.85	17.94 ± 0.49	10.17 ± 1.51	0.15 ± 0.02	2.35 ± 0.35
1055+20	1.111	399	0.88 ± 0.07	0.52 ± 0.11	6.35 ± 1.97	14.35 ± 2.32	12.87 ± 2.77	0.20 ± 0.04	2.60 ± 0.56
1354+19	0.720	376	0.59 ± 0.05	0.23 ± 0.03	12.89 ± 1.04	21.52 ± 0.95	17.23 ± 1.42	0.41 ± 0.03	5.24 ± 0.43
1548+11	1.901	379	0.89 ± 0.13	0.33 ± 0.04	6.06 ± 3.80	18.69 ± 1.02	17.68 ± 1.69	0.15 ± 0.01	1.89 ± 0.18
1618+17	0.555	430	0.84 ± 0.05	0.62 ± 0.03	7.41 ± 1.27	12.27 ± 0.62	9.78 ± 1.24	0.26 ± 0.03	3.64 ± 0.46
1830+28	0.594	217	0.81 ± 0.03	0.75 ± 0.04	8.15 ± 0.72	9.52 ± 0.88	4.92 ± 2.08	0.18 ± 0.07	1.74 ± 0.74
2325+29	1.015	425	0.83 ± 0.05	0.60 ± 0.04	7.66 ± 1.24	12.69 ± 0.83	10.11 ± 1.40	0.16 ± 0.02	2.24 ± 0.31

high redshift assuming uniform thermal electron density. In Table 1, we do this calculation for all the 31 sources studied by Garrington et al. (1991) with varying path lengths ($L \sim$ projected linear size, LS in Table 1) and two different thermal electron density models (uniform n_e and n_e following the King profile). For the uniform n_e case, we assume n_e to be 10^{-2} cm^{-3} and for the King profile case, we assume n_e at radius $r = 0$ to be 10^{-2} cm^{-3} and the core radius $a = 3 \text{ kpc}$ (see Tab. 4 in Garrington & Conway 1991). For both cases, we assume the magnetic field correlation length $\ell_b = 100 \text{ pc}$ (as expected from the fluctuation dynamo action). The estimated magnetic field for the uniform n_e case $b_{rms}(uni)$ and

that at around $r = 0$ for the King profile case $b_{rms}(KP, r = 0)$ is given in the last two columns of Table 1. The rms magnetic field for the uniform n_e case ranges from $0.14 \mu\text{G}$ to $1.33 \mu\text{G}$ and for the King profile case ranges from $1.36 \mu\text{G}$ to $6.21 \mu\text{G}$. The magnetic field strengths in the sample roughly agrees with the estimated value in Sec. 2.3. We propagate the uncertainties reported in the observed values of the depolarization fraction (Garrington et al. 1991) to magnetic field strengths. The uncertainties in field strengths ranges from 5% to 42%. The uncertainty reported here is due to the measurement error, there can be additional systematics due to variations in ℓ_b . Fig. 6 (a) and Fig. 7 (a) shows a histogram

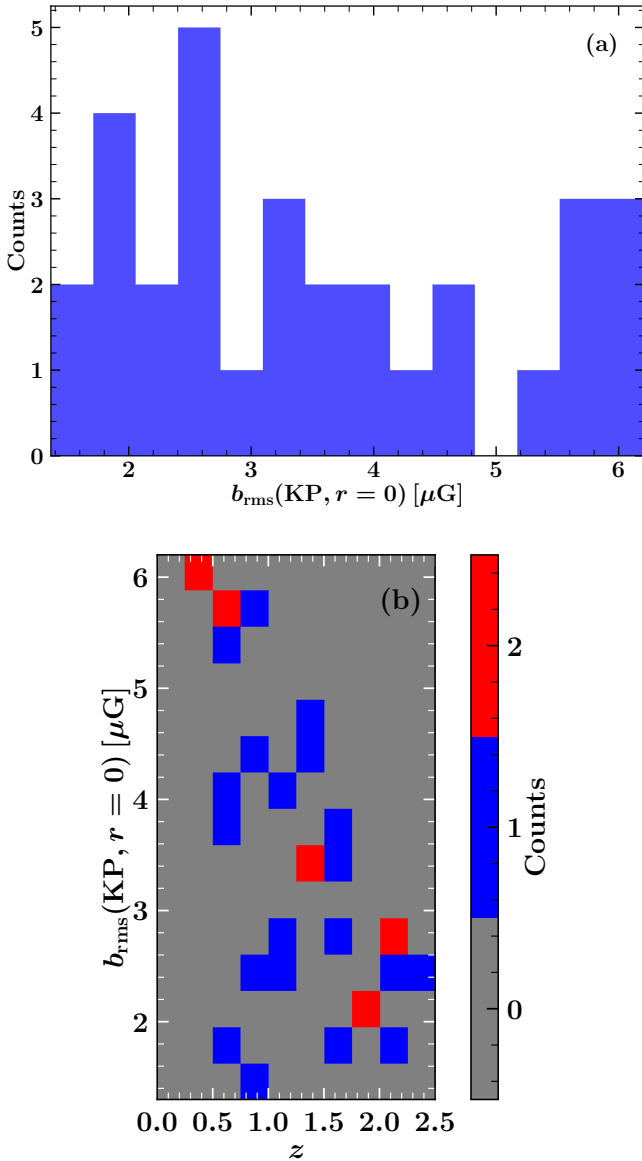


Figure 7. (a) Histogram of rms magnetic field strength $b_{\text{rms}}(\text{KP}, r=0)$ [μG] obtained from the asymmetry in polarization properties of jets from sources associated with elliptical galaxies assuming the King profile for the thermal electron density with the core radius $a = 3$ kpc and the number density at $r = 0$ as $n_e(r=0) = 10^{-2} \text{ cm}^{-3}$. (b) Two-dimensional histogram of the redshift of the sources z and $b_{\text{rms}}(\text{KP}, r=0)$. At lower z , b_{rms} tends to be somewhat (factor 2–3) higher than at higher z , although there is significant scatter in the intermediate redshift range, $0.5 \leq z \leq 1.75$.

of magnetic fields strengths in host ellipticals obtained using $b_{\text{rms}}(\text{uni})$ and $b_{\text{rms}}(\text{KP}, r=0)$ (last two columns of Table 1). Fig. 6 (b) and Fig. 7 (b) show two-dimensional histograms of the calculated magnetic field versus redshift. From the two-dimensional histograms, it appears that the magnetic field is somewhat stronger in elliptical galaxies at lower redshifts. However, we caution that the sample size is small and has

not been controlled for any selection biases. The typical strengths are broadly consistent with the simulated values shown in Fig. 1 (also in agreement with small-scale simulations in Sec. 4.), which is an encouraging sign. However, a direct comparison of the redshift trends is not possible, as the observed sample is small and its volume completeness is difficult to judge.

The Laing-Garrington effect can only be employed for elliptical galaxies with an active galactic nucleus (AGN). The jets might contaminate the radio signal as well as the turbulence and magnetic fields in such ellipticals. Thus, it may not be trivial to disentangle the influence of the jet from the magnetic field properties that would arise purely under the influence of supernova driven turbulence in the hot ISM of elliptical galaxies. In general for ellipticals with an AGN at the center, the galaxy+jet system can give rise to large-scale RM gradients and asymmetric RM distributions with non-zero mean RM (as shown in Fig. 8 of Laing et al. 2008, in comparison to our Fig. 4). Although the magnetic field strength obtained from the fluctuation dynamo analysis in quiescent ellipticals (Sec. 2) and that using the Laing-Garrington effect for ellipticals with jets are similar, the correlation scale of the magnetic field can be widely different for the two cases. Moreover, the depolarization asymmetry in jets can also be due to an extended disk of magneto-ionic medium surrounding elliptical galaxies (Gopal-Krishna & Nath 1997), absence of a spherically symmetric halo (Laing et al. 2008) or difference in Faraday rotation due to shocked and un-shocked medium (Guidetti et al. 2012). To robustly study fluctuation dynamos in elliptical galaxies using the Laing-Garrington effect, a statistically large sample of sources may be required.

5.3. Synchrotron Emission

The detection of radio synchrotron radiation could be attempted. We are interested in estimating the synchrotron flux in quiescent elliptical galaxies for which the contribution due to star formation is negligible and that due to the central AGN is absent. Assuming that there is a significant population of relativistic electrons, the flux density from the central region of an elliptical galaxy can be estimated by considering the relationship between minimum energy magnetic field strength and radio luminosity for a spherical radio source. Following Pacholczyk (1970), assuming an unresolved source with spectral index $S_\nu \propto \nu^{-0.8}$ over frequencies between 10 MHz to 100 GHz, and assuming an ion to electron energy density ratio of 100, the predicted spectral flux density is approximately

$$12 \text{ nJy} \left(\frac{b_{\text{rms}}}{1 \mu\text{G}} \right)^{3.5} \left(\frac{R}{1 \text{ kpc}} \right)^3 \left(\frac{\nu}{1 \text{ GHz}} \right)^{-0.8} \left(\frac{D_L}{100 \text{ Mpc}} \right)^{-2}, \quad (20)$$

where R is the volume radius, ν is the observing frequency, and D_L is the luminosity distance. Assuming $\nu = 100$ MHz,

$R = 1$ kpc from earlier, $b_{\text{rms}} \approx 0.5 \mu\text{G}$ from Sec. 2.3, and a distance of 50 Mpc ($z \approx 0.01$), this equates to approximately 25 nJy which is unlikely to be feasible with even the next generation of radio telescopes. However, it is plausible that this could be detected by stacking the radio emission over a large sample of suitably selected elliptical galaxies.

In apparent contrast with the flux density estimate above, Nyland et al. (2017) found that cores of early-type galaxies are bright in synchrotron because stars are still being formed in the central regions of the galaxies. They also found a deficiency in radio emission compared to the infrared emission. One possible explanation for this deficiency is the presence of significant magnetic field strengths in the medium⁶. Nyland et al. (2017) estimated magnetic fields in the range 4–85 μG , with median of 15 μG (an order of magnitude higher than that in the nearby spiral galaxies), but to estimate the magnetic field strength they assumed that those early type galaxies are very similar to present day spiral galaxies. Their assumptions included energy equipartition between cosmic rays and magnetic fields (see Seta & Beck (2019) for pros and cons of the equipartition assumption), ratio of number density of cosmic ray protons to cosmic ray electrons of 100, and disc-like or cylindrical geometry of the synchrotron emitting region with gas scale heights similar to a spiral galaxy. Additionally, the emission due to accretion by the central black hole might also contaminate the total synchrotron intensity. Based on our simple estimates from Sec. 2.3 and the indirect observational result from Section 5.2, we argue that magnetic field strengths in elliptical galaxies are probably an order of magnitude lower than that in spirals and certainly not higher.

5.4. Gravitational Lensing

Strong gravitational lens systems could be used to measure differences in RM or depolarization between multiple (and/or possibly spatially resolved) images of a background polarized radio source that have been lensed by a foreground elliptical galaxy (Greenfield et al. 1985; Patnaik et al. 1999; Narasimha & Chitre 2004)⁷. A mass model for the lensing system is required. A complication with this approach is that the local group or cluster environment will also contribute toward σ_{RM} .

Greenfield et al. (1985) studied the radio polarization signal from two gravitationally lensed images of the quasar 0957+561 ($z \approx 1.41$) at multiple wavelengths and found that the rotation measures of the two images differ by 100 rad m^{-2} . This difference can be attributed to the magnetic field in the ISM of the lensing (cD) galaxy at $z \approx 0.36$. So, to estimate

the magnetic field in the galaxy using Eq. 9 for the quasar at a redshift z , we can write RM in terms of mean quantities as

$$\text{RM} \approx \left(0.81 \frac{\langle n_e \rangle \langle b \rangle L}{\text{cm}^{-3} \mu\text{G pc}} \right) / (1+z)^2, \quad (21)$$

where $\langle \dots \rangle$ denotes the average over the path length. Assuming $\langle n_e \rangle \approx 0.01 \text{ cm}^{-3}$ and $L \approx 30$ kpc, for $\text{RM} = 100 \text{ rad m}^{-2}$ and $z = 1.41$, we obtain $\langle b \rangle \approx 2.5 \mu\text{G}$. This is comparable in strength to magnetic fields observed in the Milky Way and nearby spiral galaxies (Fletcher 2010; Haverkorn 2015; Beck 2016). Also, since the $\langle b \rangle$ is not close to zero, it refers to the presence of a large-scale or ordered field. Furthermore, such strong ordered fields are not expected in cD galaxies, and thus, the RM difference cannot be completely associated with the galaxy. The non-zero strong ordered field could be due to the contribution from the cluster’s magnetic field, which even if random (on scales of 10 kpc, Subramanian et al. 2006), can act as a coherent field over the scale of the galaxy. This argument is supported by the mass modelling of the system, which suggests that the lens must also have some contribution from the cluster to explain the lensing observations (Greenfield et al. 1985). Thus, it then becomes difficult to differentiate between the contribution to the RM difference due to the galaxy’s and cluster’s magnetic fields.

Alternatively, rather than examining RMs directly, RM variance could be probed by observing depolarization similar to Section 5.2 but over the spatial extent of the foreground lensing elliptical galaxy within an extended background radio source (Strom & Jaegers 1988; Laing 1988; Garrington et al. 1988). More recent attempts to statistically measure RM excess due to intervening galaxies (Farnes et al. 2014; Malik et al. 2020; Lan & Prochaska 2020) can also be extended to study magnetic fields in elliptical galaxies by considering the morphology of the intervening galaxies in the statistical sample.

5.5. Selection Effects

Observations must carefully consider selection effects so as to minimize potential bias from coherent magnetic fields and from unrelated RM fluctuations. The observations should ideally target giant (core) ellipticals that as a class exhibit negligible rotation (Kormendy et al. 2009). These galaxies are typically located within the central regions of clusters, so it will be important to discriminate between RM fluctuations arising in the interstellar and intracluster gas (Baldry et al. 2006; Kraljic et al. 2018). Selection should also ideally target ellipticals in hydrostatic equilibrium (Statler 2012; Penoyre et al. 2017). Note that a simple selection on red galaxies could lead to misleading results (e.g. Evans et al. 2018). Evolution with redshift in the source sample (van Dokkum et al. 2010; Penoyre et al. 2017) will need to be taken into account when compiling statistics on saturation RM variance.

⁶ Another proposed explanation was the quick escape of cosmic ray electrons. However, there is no sign of an outflow or wind in such galaxies. Thus, the cosmic rays transport must be dictated by magnetic fields.

⁷ Such an approach is shown to be successful for spiral galaxies in Mao et al. (2017).

Some of the approaches described in the sections above could be tested now using a combination of data from surveys such as the SDSS (York et al. 2000) and NVSS (Condon et al. 1998), or in the near future, for example using forthcoming data from the VLA Sky Survey (Lacy et al. 2019) and eventually from the Square Kilometre Array (Taylor et al. 2015).

6. CONCLUSIONS

We propose that observations of magnetic fields in *quiescent* elliptical galaxies would provide a direct confirmation of the operation of a fluctuation dynamo. We demonstrate that the turbulence driven by Type Ia supernova explosions in elliptical galaxies would generate magnetic fields of a sufficient strength ($0.2 - 1 \mu\text{G}$) to be observable. We examine observational prospects for measuring the magnetic saturation state of fluctuation dynamos using elliptical galaxies. We take the first steps toward characterizing the properties of magnetic fields in elliptical galaxies and analyzing historical observations of the Laing-Garrington effect to estimate magnetic field strengths in a small sample of host galaxies (Table 1). We obtain magnetic field strengths in those host galaxies lies in the range $0.14 - 1.33 \mu\text{G}$ if a uniform thermal electron density is assumed and $1.36 - 6.21 \mu\text{G}$ if the King profile for the thermal electron density is assumed. We also examine the redshift dependence of the observed magnetic field strengths (Fig. 6(b) and Fig. 7(b)) and find that on average, the magnetic field increases by a factor of 2–3 as the redshift decreases, but it is difficult to draw robust conclusions from the small sample. More generally, we also show that fluctuations in rotation measures from background polarized sources must not directly be associated with the fluctuations

in the magnetic fields as that holds true only for uniform or very weakly varying thermal electron number density.

If the proposed observations of magnetic fields in elliptical galaxies reveal much lower saturation magnetic field strengths than our estimate, this would imply gaps in our theoretical understanding of fluctuation dynamos, and would also imply that the mean-field dynamo in spiral galaxies are probably seeded with a weaker magnetic field. This in turn would require a much more efficient mean-field dynamo mechanism than presently known to explain the observed magnetic fields in the Milky Way and nearby spiral galaxies.

We thank the anonymous referee for a thorough review of this work. AS thanks Andrew Fletcher, Sui Ann Mao, Anvar Shukurov, Kandaswamy Subramanian, and Rainer Beck for very useful discussions. AS thanks Govind Nandakumar for a useful discussion on error analysis. We thank Sharanya Sur for providing valuable comments on the paper. LFSR acknowledges funding from the European Research Council (ERC) under the European Union’s Horizon 2020 research and innovation programme (grant agreement No 772663). CF acknowledges funding provided by the Australian Research Council (Discovery Project DP170100603 and Future Fellowship FT180100495), and the Australia-Germany Joint Research Cooperation Scheme (UA-DAAD). CAH acknowledges support from the European Union’s Horizon 2020 research and innovation programme under the Marie Skłodowska-Curie grant agreement No 705332. We further acknowledge high-performance computing resources provided by the Leibniz Rechenzentrum and the Gauss Centre for Supercomputing (grants pr32lo, pr48pi and GCS Large-scale project 10391), the Australian National Computational Infrastructure (grant ek9) in the framework of the National Computational Merit Allocation Scheme and the ANU Allocation Scheme.

REFERENCES

- Anderson, C. S., Gaensler, B. M., Feain, I. J., & Franzen, T. M. O. 2015, *Astrophys. J.*, 815, 49
- Arshakian, T. G., Beck, R., Krause, M., & Sokoloff, D. 2009, *Astron. Astrophys.*, 494, 21
- Baldry, I. K., Balogh, M. L., Bower, R. G., et al. 2006, *Mon. Not. R. Astron. Soc.*, 373, 469
- Basu, A., Fletcher, A., Mao, S. A., et al. 2019, *Galaxies*, 7, 89
- Beck, R. 2016, *Ann. Rev. Astron. Astrophys.*, 24, 4
- Beck, R., Brandenburg, A., Moss, D., Shukurov, A., & Sokoloff, D. 1996, *Ann. Rev. Astron. Astrophys.*, 34, 155
- Benson, A. J., & Devereux, N. 2010, *Mon. Not. R. Astron. Soc.*, 402, 2321
- Bhat, P., & Subramanian, K. 2013, *Mon. Not. R. Astron. Soc.*, 429, 2469
- Brandenburg, A., & Subramanian, K. 2005, *Phys. Rep.*, 417, 1
- Bregman, J. N., Miller, E. D., Athey, A. E., & Irwin, J. A. 2005, *Astrophys. J.*, 635, 1031
- Bregman, J. N., Miller, E. D., & Irwin, J. A. 2001, *Astrophys. J. Lett.*, 553, L125
- Burn, B. J. 1966, *Mon. Not. R. Astron. Soc.*, 133, 67
- Cappellari, M., Emsellem, E., Krajnović, D., et al. 2011, *Mon. Not. R. Astron. Soc.*, 416, 1680
- Cappellaro, E., Evans, R., & Turatto, M. 1999, *Astron. Astrophys.*, 351, 459

- CHIME/FRB Collaboration, Amiri, M., Bandura, K., et al. 2019, *Nature*, 566, 230
- Condon, J. J., Cotton, W. D., Greisen, E. W., et al. 1998, *AJ*, 115, 1693
- Cordes, J. M., & Chatterjee, S. 2019, *Ann. Rev. Astron. Astrophys.*, 57, 417
- de Plaa, J., Zhuravleva, I., Werner, N., et al. 2012, *Astron. Astrophys.*, 539, A34
- Dyson, J. E., & Williams, D. A. 1997, *The physics of the interstellar medium*, 2nd edn. (CRC Press), doi:10.1201/9780585368115
- Emsellem, E., Cappellari, M., Krajnović, D., et al. 2011, *Mon. Not. R. Astron. Soc.*, 414, 888
- Enßlin, T. A., & Vogt, C. 2003, *Astron. Astrophys.*, 401, 835
- Evans, F. A., Parker, L. C., & Roberts, I. D. 2018, *Mon. Not. R. Astron. Soc.*, 476, 5284
- Fabian, A. C. 1994, *Annual Review of Astronomy and Astrophysics*, 32, 277
- Fabian, A. C., Reynolds, C. S., Taylor, G. B., & Dunn, R. J. H. 2005, *Mon. Not. R. Astron. Soc.*, 363, 891
- Farnes, J. S., O’Sullivan, S. P., Corrigan, M. E., & Gaensler, B. M. 2014, *Astrophys. J.*, 795, 63
- Federrath, C. 2016, *Journal of Plasma Physics*, 82, 535820601
- Federrath, C., Chabrier, G., Schober, J., et al. 2011, *Phys. Rev. Lett.*, 107, 114504
- Federrath, C., Klessen, R. S., & Schmidt, W. 2009, *Astrophys. J.*, 692, 364
- Federrath, C., Schober, J., Bovino, S., & Schleicher, D. R. G. 2014, *Astrophys. J.*, 797, L19
- Felten, J. E. 1996, *Astronomical Society of the Pacific Conference Series*, Vol. 88, *Mitigating the Baryon Crisis in Clusters: Can Magnetic Pressure be Important?*, ed. V. Trimble & A. Reisenegger, 271
- Fletcher, A. 2010, in *The Dynamic Interstellar Medium: A Celebration of the Canadian Galactic Plane Survey*, ed. R. Kothés, T. L. Landecker, & A. G. Willis, Vol. 438, 197
- Fletcher, A., Beck, R., Shukurov, A., Berkhuijsen, E. M., & Horellou, C. 2011, *Mon. Not. R. Astron. Soc.*, 412, 2396
- Forman, W., Jones, C., & Tucker, W. 1985, *Astrophys. J.*, 293, 102
- Gaensler, B. M., Haverkorn, M., Staveley-Smith, L., et al. 2005, *Science*, 307, 1610
- Garrington, S. T., & Conway, R. G. 1991, *Mon. Not. R. Astron. Soc.*, 250, 198
- Garrington, S. T., Conway, R. G., & Leahy, J. P. 1991, *Mon. Not. R. Astron. Soc.*, 250, 171
- Garrington, S. T., Leahy, J. P., Conway, R. G., & Laing, R. A. 1988, *Nature*, 331, 147
- Gopal-Krishna, & Nath, B. B. 1997, *Astron. Astrophys.*, 326, 45
- Greenfield, P. D., Roberts, D. H., & Burke, B. F. 1985, *Astrophys. J.*, 293, 370
- Guidetti, D., Laing, R. A., Croston, J. H., Bridle, A. H., & Parma, P. 2012, *Mon. Not. R. Astron. Soc.*, 423, 1335
- Hales, C. A. 2013, *ArXiv e-prints*, arXiv:1312.4602
- Hales, C. A., Norris, R. P., Gaensler, B. M., & Middelberg, E. 2014, *Mon. Not. R. Astron. Soc.*, 440, 3113
- Haugen, N. E., Brandenburg, A., & Dobler, W. 2004, *Phys. Rev. E*, 70, 016308
- Haverkorn, M. 2015, in *Astrophysics and Space Science Library*, Vol. 407, *Magnetic Fields in Diffuse Media*, ed. A. Lazarian, E. M. de Gouveia Dal Pino, & C. Melioli, 483
- Haverkorn, M., Brown, J. C., Gaensler, B. M., & McClure-Griffiths, N. M. 2008, *Astrophys. J.*, 680, 362
- Hernquist, L. 1990, *Astrophys. J.*, 356, 359
- Hollins, J. F., Sarson, G. R., Shukurov, A., Fletcher, A., & Gent, F. A. 2017, *Astrophys. J.*, 850, 4
- Houde, M., Fletcher, A., Beck, R., et al. 2013, *Astrophys. J.*, 766, 49
- Iacobelli, M., Haverkorn, M., Orrù, E., et al. 2013, *Astron. Astrophys.*, 558, A72
- Kim, K. S., Lilly, S. J., Miniati, F., et al. 2016, *Astrophys. J.*, 829, 133
- Kormendy, J., Fisher, D. B., Cornell, M. E., & Bender, R. 2009, *ApJS*, 182, 216
- Kraljic, K., Arnouts, S., Pichon, C., et al. 2018, *Mon. Not. R. Astron. Soc.*, 474, 547
- Lacey, C. G., Baugh, C. M., Frenk, C. S., et al. 2016, *Mon. Not. R. Astron. Soc.*, 462, 3854
- Lacy, M., Baum, S. A., Chandler, C. J., et al. 2019, *arXiv e-prints*, arXiv:1907.01981
- Laing, R. A. 1988, *Nature*, 331, 149
- Laing, R. A., Bridle, A. H., Parma, P., & Murgia, M. 2008, *Mon. Not. R. Astron. Soc.*, 391, 521
- Lan, T.-W., & Prochaska, J. X. 2020, *Mon. Not. R. Astron. Soc.*, 496, 3142
- Li, M., Li, Y., Bryan, G. L., Ostriker, E. C., & Quataert, E. 2019, *arXiv e-prints*, arXiv:1909.04204
- , 2020, *Astrophys. J.*, 894, 44
- Mac Low, M.-M., & Klessen, R. S. 2004, *Reviews of Modern Physics*, 76, 125
- Mac Low, M.-M., Klessen, R. S., Burkert, A., & Smith, M. D. 1998, *Phys. Rev. Lett.*, 80, 2754
- Malik, S., Chand, H., & Seshadri, T. R. 2020, *Astrophys. J.*, 890, 132
- Mao, S. A., Carilli, C., Gaensler, B. M., et al. 2017, *Nature Astronomy*, 1, 621
- Mathews, W. G., & Brighenti, F. 1997, *Astrophys. J.*, 488, 595
- , 2003, *Annual Review of Astronomy and Astrophysics*, 41, 191
- Metzger, B. D., Margalit, B., & Sironi, L. 2019, *Mon. Not. R. Astron. Soc.*, 485, 4091
- Minter, A. H., & Spangler, S. R. 1996, *Astrophys. J.*, 458, 194

- Monin, A. S., & Yaglom, A. M. 1971, *Statistical Fluid Mechanics* (Cambridge, Massachusetts, USA: MIT Press)
- Moss, D., & Shukurov, A. 1996, *Mon. Not. R. Astron. Soc.*, 279, 229
- Murgia, M., Govoni, F., Feretti, L., et al. 2004, *Astron. Astrophys.*, 424, 429
- Narasimha, D., & Chitre, S. M. 2004, *Journal of Korean Astronomical Society*, 37, 355
- Nyland, K., Young, L. M., Wrobel, J. M., et al. 2017, *Mon. Not. R. Astron. Soc.*, 464, 1029
- Ogorzalek, A., Zhuravleva, I., Allen, S. W., et al. 2017, *Mon. Not. R. Astron. Soc.*, 472, 1659
- Ohno, H., & Shibata, S. 1993, *Mon. Not. R. Astron. Soc.*, 262, 953
- Ostriker, J. P., & McKee, C. F. 1988, *Reviews of Modern Physics*, 60, 1
- O'Sullivan, E., Forbes, D. A., & Ponman, T. J. 2001, *Mon. Not. R. Astron. Soc.*, 328, 461
- Pacholczyk, A. G. 1970, *Radio astrophysics. Nonthermal processes in galactic and extragalactic sources* (San Francisco: Freeman)
- Patnaik, A. R., Kembal, A. J., Porcas, R. W., & Garrett, M. A. 1999, *Mon. Not. R. Astron. Soc.*, 307, L1
- Penoyre, Z., Moster, B. P., Sijacki, D., & Genel, S. 2017, *Mon. Not. R. Astron. Soc.*, 468, 3883
- Petroff, E., Hessels, J. W. T., & Lorimer, D. R. 2019, *A&A Rv*, 27, 4
- Price, D. J., Federrath, C., & Brunt, C. M. 2011, *Astrophys. J. Lett.*, 727, L21
- Rincon, F. 2019, *Journal of Plasma Physics*, 85, 205850401
- Ruzmaikin, A. A., Sokoloff, D. D., & Shukurov, A. M., eds. 1988, *Astrophysics and Space Science Library*, Vol. 133, *Magnetic fields of galaxies*
- Schekochihin, A. A., Cowley, S. C., Hammett, G. W., Maron, J. L., & McWilliams, J. C. 2002, *New Journal of Physics*, 4, 84
- Schekochihin, A. A., Cowley, S. C., Taylor, S. F., Maron, J. L., & McWilliams, J. C. 2004, *Astrophys. J.*, 612, 276
- Seta, A. 2019, PhD thesis, Newcastle University, Newcastle Upon Tyne, UK. <http://theses.ncl.ac.uk/jspui/handle/10443/4685>
- Seta, A., & Beck, R. 2019, *Galaxies*, 7, 45
- Seta, A., Bhat, P., & Subramanian, K. 2015, *Journal of Plasma Physics*, 81, 395810503
- Seta, A., Bushby, P. J., Shukurov, A., & Wood, T. S. 2020, *Physical Review Fluids*, 5, 043702
- Seta, A., Shukurov, A., Wood, T. S., Bushby, P. J., & Snodin, A. P. 2018, *Mon. Not. R. Astron. Soc.*, 473, 4544
- Shukurov, A. 2004, *ArXiv Astrophysics e-prints*, astro-ph/0411739
- Shukurov, A., Snodin, A. P., Seta, A., Bushby, P. J., & Wood, T. S. 2017, *Astrophys. J. Lett.*, 839, L16
- Shukurov, A., & Sokoloff, D. 2007, in *Les Houches, Session LXXXVIII, Dynamos*, ed. P. Cardin & L. F. Cugliandolo, Vol. 88 (Amsterdam: Elsevier), 251–299. [http://dx.doi.org/10.1016/S0924-8099\(08\)80008-X](http://dx.doi.org/10.1016/S0924-8099(08)80008-X)
- Sokoloff, D. D., Bykov, A. A., Shukurov, A., et al. 1998, *Mon. Not. R. Astron. Soc.*, 299, 189
- Statler, T. S. 2012, in *Astrophysics and Space Science Library*, Vol. 378, *Astrophysics and Space Science Library*, ed. D.-W. Kim & S. Pellegrini, 207
- Stone, J. M., Ostriker, E. C., & Gammie, C. F. 1998, *Astrophys. J. Lett.*, 508, L99
- Strom, R. G., & Jaegers, W. J. 1988, *Astron. Astrophys.*, 194, 79
- Subramanian, K. 1999, *Phys. Rev. Lett.*, 83, 2957
- Subramanian, K., Shukurov, A., & Haugen, N. E. L. 2006, *Mon. Not. R. Astron. Soc.*, 366, 1437
- Sur, S. 2019, *Mon. Not. R. Astron. Soc.*, 488, 3439
- Taylor, R., Agudo, I., Akahori, T., et al. 2015, in *Advancing Astrophysics with the Square Kilometre Array (AASKA14)*, 113
- Tobias, S. M., Cattaneo, F., & Boldyrev, S. 2011, *ArXiv e-prints*, arXiv:1103.3138
- Tzeferacos, P., Rigby, A., Bott, A. F. A., et al. 2018, *Nature Communications*, 9, 591
- van Dokkum, P. G., Whitaker, K. E., Brammer, G., et al. 2010, *Astrophys. J.*, 709, 1018
- Wilkin, S. L., Barengi, C. F., & Shukurov, A. 2007, *Phys. Rev. Lett.*, 99, 134501
- York, D. G., Adelman, J., Anderson, Jr., J. E., et al. 2000, *AJ*, 120, 1579
- Zeldovich, Ya. B., Ruzmaikin, A. A., & Sokoloff, D. D. 1990, *The Almighty Chance* (Singapore: World Scientific)
- Zweibel, E. G. 2020, *Astrophys. J.*, 890, 67